Physics-based Compact Model of Integrated Gate-Commutated Thyristor with Multiple Effects for High Power Application

Gang Lyu[1], Chijie Zhuan[1], Rong Zeng[1*], Teng Long[2], Patrick Palmer[2]

[1]Department of Electrical Engineering, Tsinghua University, Beijing, China
[2]Department of Electrical Engineering, University of Cambridge, Cambridge, UK
*zengrong@tsinghua.edu.cn

Abstract: This paper presents a physics-based compact model of integrated gate-commutated thyristor (IGCT) with multiple effects for high power application. The proposed model has both acceptable accuracy and computation time requirement, which is suitable for system level circuit simulation and IGCT's whole wafer modelling work. First, the development of IGCT model is discussed and the one-dimension phenomenon of IGCT is analyzed in the paper. Second, a physics-based compact model of IGCT is proposed. The proposed model of IGCT includes multiple physical effects that are crucial to IGCTs working in high power applications. These physical effects include the impact ionization effect, moving boundary of depletion region during punch-thourgh (PT) and the local lifetime region. The Fourier series solution is applied for the ambipolar diffusion equation in the base region. Third, the proposed model is implemented in Simulink and compared with the model in Silvaco Atlas, a finite-element (FEM) tool. Finally, the proposed compact model of IGCT is validated by experiments.

Keywords—physics-based compact model, local lifetime region, gate commutated thyristors, punch through, power semiconductor modeling

NOMENCLATURE

A	Total active area. (cm^2)
q	Electric charge (J)
ε_{Si}	Dielectric constant for silicon. (F/cm^2)
k	Boltzmann's constant. (J/K)
T	Absolute temperature. (K)
$V_t=kT/q$	Thermal Voltage. (V)
μ_{n0}	Electron mobility. (cm^2/Vs)
μ_{p0}	Hole mobility. (cm^2/Vs)
D	Ambipoar diffusivity. (cm^2/s)
D_n	Electron diffusivity. (cm^2/s)
D_p	Hole diffusivity. (cm^2/s)
h	Recombination parameter. (cm^2)
J	Current density. (A/cm^2)
I_{n1},I_{p1}	Electron and hole current at x_1 edge of undepleted drift region. (A)
I_{n2},I_{p2}	Electron and hole current at x_2 edge of undepleted drift region. (A)
I_A	Total anode current. (A)
I_C	Total cathode current. (A)
I_G	Total gate current. (A)
N_B	N-base region doping concentration. (cm^{-3})
N_{Pb}	P-base region doping concentration. (cm^{-3})
N_{Nb}	N-base region doping concentration. (cm^{-3})
n_i	Intrinsic carrier concentration. (cm^{-3})
n	Electron carrier concentration. (cm^{-3})
p	Hole carrier concentration. (cm^{-3})
p_{x1}	Hole carrier density at x_1. (cm^{-3})
p_{x2}	Hole carrier density at x_2. (cm^{-3})
t	Time. (μs)
τ_{HL}	High-level lifetime. (μs)
τ_{LL}	Low-level lifetime. (μs)
V_d	Voltage across depletion region. (V)
W	Thickness of stored charge region. (cm)
W_B	Thickness of N-base region. (cm)
W_{N+}	Thickness of N-base region. (cm)
W_{Pb}	Thickness of P-base region. (cm)
W_{Nb}	Thickness of N-buffer region. (cm)

1. Introduction

In recent years, the integrated gate-commutated thyristor (IGCT) has gained extended attentions especially in high power operation conditions due to their superior features, including: 1) large safe operation area (SOA); 2) lower on state loss; 3) higher thermal capacity and better cooling capacity due to press pack package; 4) better ruggedness. Thus IGCT has been applied in many high power apparatus such as hybrid circuit breakers, statcom and multilevel converters [1]-[4].

For the purpose of circuit design and device design, models of high power IGCT are greatly desired for accurately prediction of IGCT's behavior. Many semiconductor models have been developed in the latest two decades as reported in literatures, and these models can be categorized into five levels based on their modelling complexity and accuracy [5], [6], summarized in Table.1.

The Level 0 models are like ideal switches without any physical features, and these models can be applied for system simulation. Models ranging in Level 1 [7]-[8] and Level 2 [9]-[11] are simplified physics-based models which are suitable for circuit design with acceptable error. However, the Level 0-2 models are too simple, leading to poor prediction of switching behaviors. The IGCT models ranging in Level 4 and Level 5 [12] are two dimensional or three dimensional models developed in finite element (FEM) tools. They are the most accurate models but great central process unit (CPU) capacity is required. The Level 4-5 models can be applied in the device design such as the doping profile calculation. However, the optimization of gate commutated thyristor's (GCT's) wafer, such as the cell arrangement optimization, can be hardly

fulfilled with the Level 4-5 models. This is because the lateral design of GCT prefers the whole wafer simulation, where very long calculation time is required due to the Level 4-5 models' complexity.

Table.1 Different Levels of Semiconductor Device Models

Level	Features	Applications
0	Static, ideal switch Very little CPU capacity	System dynamics where many switching cycles must be simulated.
1	Basic static & dynamic characteristics within SOA, little CPU capacity	General use where approximate waveform accuracy is satisfactory.
2	Simplified physics-based model such as lumped-charge model, can be nonlinear; little CPU capacity	Prediction of switching waveform with acceptable error
3	Physics-based compact model, usually one-dimension, accurate characteristics within SOA; Acceptable CPU capacity	Snubber and gate drive design. Heat sink design Thermal stress and instabilities. Circuit optimization. Whole wafer lateral optimization.
4	Two- or three- dimension finite-element model All the relevant physics; Very long computation time	Accurate performance prediction Design of GCT cell
5	Operation outside SOA including failure mode Degradation effect on electrical and thermal characteristics; Radiation dose Very long computation time	Device failure Second breakdown Prompt radiation effect Performance degradation.

The Level 3 models are physics-based compact models with accurate characteristics within SOA and acceptable CPU capacity. So the Level 3 models are suitable for circuit design optimization where the prediction of the IGCT' electrical characteristics is required such as switching loss and voltage overshoot during turning off [12]. In addition, with acceptable CPU capacity requirement, the Level 3 models can also be used to simulate the whole GCT wafer where optimization of the layout of GCT wafer can be fulfilled.

However, some particular physical characteristics have not been captured by the existing Level 3 models of IGCTs. The impact ionization effect needs to be modelled when IGCT block high voltage with an inductive load. Only when the impact ionization effect is included, the switching characteristics especially the thermal performance and overvoltage during turning off can be predicted correctly. And the moving boundary of the buffer region due to punch-through (PT) effect in high-power IGCTs has neither been properly reported nor well considered in existing literatures [14-17]. Reported approaches of PT effect in existing IGBT models, however, have the buffer region modelled as a lumped-charge region with fixed boundary [17], which is not physically correct during punch-through. In addition, as reported in [19], local lifetime region has been applied in some IGCTs for the purpose of reducing switching losses, which has not been considered in existing Level-3 models.

This paper describes the development of a Level 3 IGCT model including the punch-through effect coupled with the impact ionization effect and local lifetime region. The modified Fourier-based model was used to solve the ambipolar diffusion equation (ADE) in carrier storage region (CSR). The depletion region is modified based on the impact ionization effect. The proposed Level 3 model has been validated by both a Level 4 model developed in Silvaco Atlas and experimental results.

2. The One-Dimension Phenomenon of GCT

A typical GCT half-cell model of Level 4 has been developed in the FEM tool of Silvaco Atlas, shown in Fig. 1 (a). Fig. 1 (b) shows a schematic diagram of GCT depicted in (a). Three P-N junctions are marked as J1~J3. During turning on, holes and electrons are injected into the N-base and P-base regions. During turning off, the cathode to gate is reverse biased by the gate drive unit. The reverse-biased voltage of cathode to gate drives the current commutates from the cathode to the gate in less than 2 μs prior to establishment of blocking voltage, shown as the current density distribution in Fig. 1 (a). This is known as the hard-drive requirement [20], which makes IGCT superior to gate turn-off thyristor (GTO) for turning off.

A schematic diagram of current path is depicted by arrows in Fig. 1 (b). During current commutating, the load current concentrates in the P+-base region, of which the thickness is 30-40 μm [20], as shown in Fig. 1 (a) and Fig. 1 (b). Thus the current is distributed in a one-dimensional area across the whole base region, except the narrow P+-base area which is close to the gate and cathode. After current commutating, in general, the GCT can be considered to have one-dimensional area for approximately 95% of the whole cross section.

The proposed one-dimensional GCT structure is shown in Fig. 1(c). In this paper, the Fourier equations are employed to solve the ambipolar diffusion equation (ADE) in carrier storage region (CSR) while local lifetime is considered. The right boundary of CSR, *x2*, is derived from the depletion region. In the depletion region, the impact ionization effect is considered in the model to precisely simulate the anode voltage waveform. Due to the comparatively narrow width and high doping of the P-base, P^+-base and N-buffer region, a charge control approach is used to describe the excess carrier behavior in those regions [14]. The moving-boundary effect of depletion region boundary during punch-through is considered in the N-buffer model to better simulate the snappy diminishing current tail. All these regions are coupled together through the current components and carrier densities at junction boundaries.

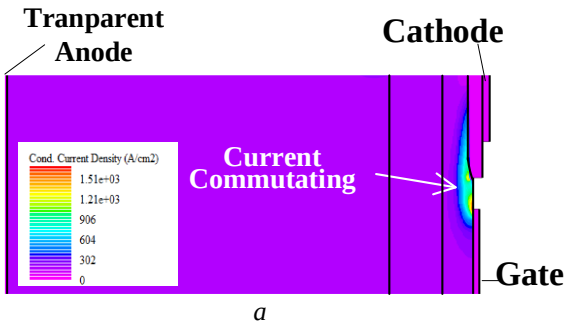

a

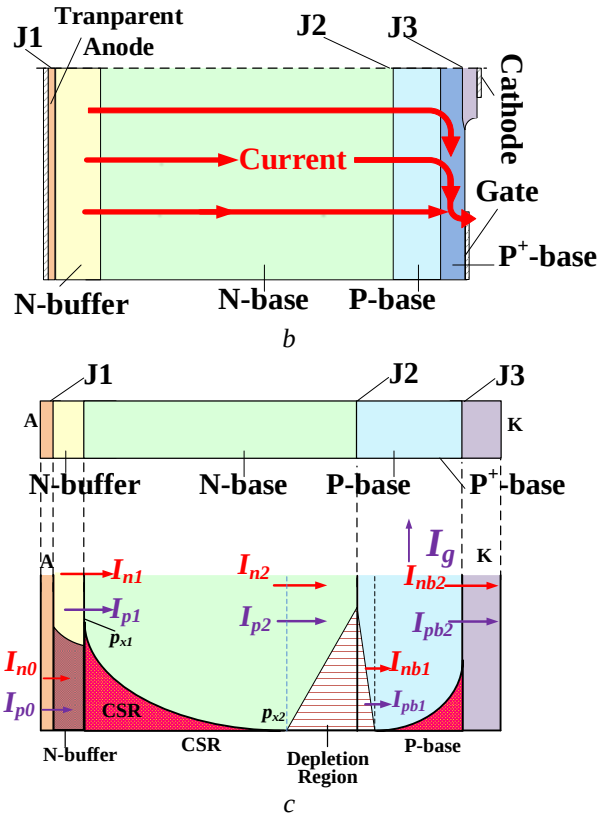

Fig. 1 . *One-dimensional phenomenon in GCT's half-cell during turning off.*
(a) Current density distribution during turning off,
(b) Schematic diagram of GCT's half-cell,
(c) Schematic diagram of one-dimensional model of GCT.

3. Model of the High Power IGCT with Multiple Physical Effects

3.1. The Normalization of Quantities in the Basic Equations

The basic equations for power semiconductor are Poisson's equation and the continuity equations:

$$\begin{cases} \nabla^2\psi = -\dfrac{Q}{\varepsilon} \\ \dfrac{\partial n}{\partial t} = \dfrac{1}{q}\dfrac{dJ_n}{dx} + G_n - R_n \\ \dfrac{\partial p}{\partial t} = -\dfrac{1}{q}\dfrac{dJ_p}{dx} + G_p - R_p \end{cases} \tag{1}$$

Many simplified forms are derived from (1), among which the ambipolar diffusion equation (ADE) is the most famous one:

$$\frac{\partial p}{\partial t} = D\frac{\partial^2 p}{\partial x^2} - \frac{p}{\tau} \tag{2}$$

The numerical values of carrier density (n, p) are several orders of magnitude larger than those of J and ψ. It is crucial to express the equations into dimensionless form to avoid stiff problem [21]. In the following context all the symbols will refer to normalized quantities according to Table.2, unless otherwise indicated. An example is given below where the ADE is normalized. The parameters with the subscript *UN* refers to the ones without normalization.

$$\frac{\partial p_{UN}}{\partial t_{UN}} = D_{UN}\frac{\partial^2 p_{UN}}{\partial x_{UN}^2} - \frac{p_{UN}}{\tau_{UN}}$$

$$\Rightarrow \frac{\partial p_{UN}/n_i}{\partial t_{UN}/(L_D^2/D_0)} = D_{UN}/D_0 \cdot \frac{\partial^2 p_{UN}/n_i}{\partial x_{UN}^2/L_D^2} - \frac{p_{UN}/n_i}{\tau_{UN}/(L_D^2/D_0)}$$

$$\Rightarrow \frac{\partial p}{\partial t} = D\frac{\partial^2 p}{\partial x^2} - \frac{p}{\tau}$$

Table.2 List of Normalization Factors for the Quantities of Interest

Description	Normalized Quantity	Normalization Factor
Position coordinate	W, W_B, W_{Pb}, W_{Nb}	$L_D = \sqrt{\varepsilon_{Si}V_t/qn_i}$
Applied Voltage	V_d	V_t
Electric field	E	V_t/L_D
Carrier density	n, p	n_i
Excess carriers	Q	$n_i q L_D^3$
Doping profile	N_B	n_i
Current density	I_n, I_p	$-qD_0n_i/L_D^2$
Carrier diffusion constants	D_n, D_p, D	$D_0=1$
Carrier mobilities	μ_n,μ_p	D_0/V_t
Lifetime	τ_{HL}, τ_{LL}	L_D^2/D_0
time	t	L_D^2/D_0

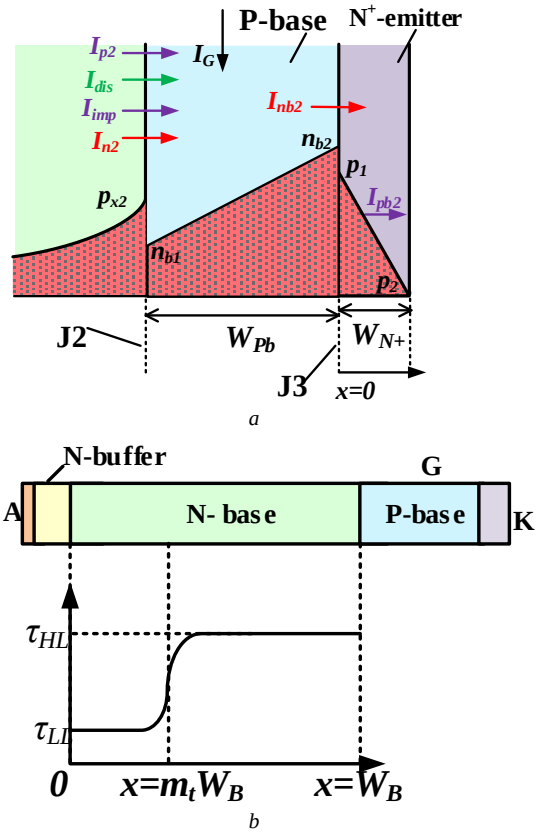

Fig. 2 . ***(a)*** *Boundary Conditions of the P-base Region,* ***(b)*** *the Layout of IGCT with Local Lifetime Region*

3.2. Model of the P-base Region with Charge Control Approach

The boundary conditions of the P-base region is shown in Fig. 2 (a). Due to the high doping profile and the thin thickness of the P-base region compared to the N-base region, the excess carriers in the P-base region can be presented as a linear distribution. The excess carriers are due to the injection of charges from the N^+-emitter and the P-N-P transistor respectively. When turning off, the excess carriers are swept out by the reverse gate current, commutating the current from the cathode to the gate. The depletion region begins to form in the vicinity of J2 after current is fully commutated to the gate, known as the hard-drive requirement. The total excess carriers in the P-base region, Q_{Pb}, can be described as:

$$\frac{dQ_{Pb}}{dt} = -\frac{Q_{Pb}}{\tau_{Pb}} + I_{p2} + I_{disp} + I_{imp} - I_{pb2} - I_G \quad (3)$$

where τ_{Pb} is the minority carrier lifetime in the P-base region. The Q_{Pb} in the P-base region can also be described by lumped charge as:

$$Q_{Pb} = \frac{qAW_{Pb}(n_{b1} + n_{b2})}{2} \quad (4)$$

The diffusion current due to the electrons in the P-base region can be described as:

$$I_{n2} = \frac{qAD_n(n_{b2} - n_{b1})}{W_{Pb}} \quad (5)$$

Using I_{n2}, the hole current at the boundary of J2 can be derived as:

$$I_{p2} = I_A - I_{disp} - I_{imp} - I_{n2} \quad (6)$$

The electron concentration at the boundary of J2 is related to the hole concentration p_{x2}. Using the Boltzmann quasi-equilibrium boundary condition for the J2 boundary, the n_{b1} can be derived as:

$$n_{b1} = \frac{p_{x2}N_B}{N_{Pb}} \quad (7)$$

Based on equations from (3) to (7), the variables I_{disp}, I_{imp}, I_G, I_{disp}, p_{x2} and V_d are all boundary conditions derived from other regions. In order to solve the equations above, the diffusive hole current in the N^+-emitter region I_{pb2} is required. Due to the high level doping profile in the N^+-emitter region, the continuity equation of holes can be expressed as:

$$\begin{cases} \dfrac{d^2p(x)}{dt^2} = \dfrac{p(x)}{D\tau_{N+}} = \dfrac{p(x)}{L_p^2} \\ p_1 = \dfrac{n_{b2}^2}{N_{N+}} \\ p_2 = 0 \end{cases} \quad (8)$$

Combine the continuity equations and its boundary conditions, I_{pb2} can be solved as the derivative of hole distribution at J3:

$$I_{pb2} = \frac{qAD_p n_{b2}^2}{L_p \tanh(W_{N+}/L_p)} \quad (9)$$

The junction voltage of J3 is calculated by using the Boltzmann quasi-equilibrium boundary condition:

$$V_{J3} = V_t \ln \frac{n_{b2}N_{Pb}}{n_i^2} \quad (10)$$

I_G continues to sweep out holes generated by the doped accepters after all the excess carriers are swept out of the P-base region. p_{b2} stops to decline until the reverse voltage of J3 becomes equal to the reverse bias gate drive voltage, resulting in $V_{J3}=V_G$.

Thus the model of P-base region is derived by combining (3) to (9).

3.3. Model of the CSR with Local Lifetime Region

It is necessary to reduce switching loss of IGCTs in applications of switching mode power converters. Local lifetime region is introduced to let IGCTs have low switching losses by applying proton irradiation [19]. Killing the carrier lifetime in the area of the N-base region near the N-buffer region reduces the turn-off loss significantly [22], [23]. This is because decreased carrier lifetime accelerates the expansion of the depletion region and shortens the tail current which needs to be swept away before the establishment of the full anode voltage. According to [22], the assumed layout of the IGCT with lifetime region are shown in Fig.2 (b), with lifetime killing taking place in the lower lifetime region (τ_L). And m_t is the coefficient of adjusting the width of the region where lifetime is killed.

The excess carrier density is described by the ADE:

$$\frac{\partial p(x,t)}{\partial t} = D\frac{\partial^2 p(x,t)}{\partial x^2} - \frac{p(x,t)}{\tau(x)} \quad (11)$$

where $p(x,t)$ is the excess carrier density. The $p(x,t)$ can be expressed as Fourier series in space x, with the coefficient p_k varying in time t:

$$\begin{cases} p(x,t) = p_0(t) + \sum_{k=1}^{\infty} p_k(t)\cos(\dfrac{k\pi(x-x_1)}{x_2-x_1}) \\ p_0(t) = \dfrac{1}{x_2-x_1}\int_{x_1}^{x_2} p(x,t)dx \\ p_k(t) = \dfrac{2}{x_2-x_1}\int_{x_1}^{x_2} p(x,t)\cos(\dfrac{k\pi(x-x_1)}{x_2-x_1})dx \end{cases} \quad (12)$$

The use of (12) separates time and space in the partial differential equation, achieving a much faster solving speed. By integrating the Fourier serious coefficients from x_1 to x_2 in the ADE, the standard solution can be found in [14].

While the standard solution of the ADE is suitable for fixed minority carrier lifetime τ, the solution for variation of τ with position must be taken into consideration as shown in Fig. 2 (b).

Assuming the lifetime $\tau(x)$ is known between $x=0$ to $x=W_B$, the reciprocal of the lifetime is expressed as a Fourier series as explained in [24]:

$$\frac{1}{\tau(x)} = \tau'(x) = \sum_{k=0}^{\infty} \tau_k'(t)\cos(\frac{k\pi(x-x_1)}{x_2-x_1}) \quad (13)$$

The reciprocal of the lifetime allows a compact solution of the ADE. This is achieved by multiplying each term in (11), ADE, by $\cos(k\pi(x-x_1)/(x_2-x_1))$. And integrating each term from x_1 to x_2 to get ADE's solution in Fourier series. Taking the lifetime term as an example:

$$\begin{aligned}&\int_{x1}^{x2} p(x,t)\sum_{k=0}^{\infty}\tau_k{}'(t)\cos(\frac{k\pi(x-x_1)}{x_2-x_1})dx\\&=\tau_0'(\frac{x_2-x_1}{2})p_k\\&\quad+\frac{\tau_k'}{2}(\frac{x_2-x_1}{2})(p_{2k}+p_0)\\&\quad+\sum_{\substack{n=1\\n\neq k}}^{\infty}\frac{\tau_n'}{2}(\frac{x_2-x_1}{2})(p_{n+k}+p_{n-k})\end{aligned}\tag{14}$$

Including τ_k' in the integration of $p/\tau(x)$ term in the ADE gives the following expressions for the calculating the Fourier coefficients:

$$\begin{cases}\text{for } k>0:\\ \frac{2D}{x_2-x_1}[\frac{\partial p}{\partial x}|_{x2}(-1)^k-\frac{\partial p}{\partial x}|_{x1}]\\ =\frac{dp_k}{dt}+p_k[\tau_0{}'+\frac{D\pi^2k^2}{(x_2-x_1)^2}]+\\ \frac{\tau_k{}'}{2}(p_{2k}+p_0)+\sum_{\substack{n=1\\n\neq k}}^{\infty}\frac{\tau_n{}'}{2}(p_{n+k}+p_{n-k})\\ \frac{2}{x_2-x_1}(\sum_{\substack{n=1\\n\neq k}}^{\infty}\frac{n^2p_n}{n^2-k^2}[\frac{dx_1}{dt}-(-1)^{n+k}\frac{dx_2}{dt}]+\frac{p_k}{4}[\frac{dx_1}{dt}-\frac{dx_2}{dt}])\\ \text{for } k=0:\\ \frac{D}{x_2-x_1}[\frac{\partial p}{\partial x}|_{x2}-\frac{\partial p}{\partial x}|_{x1}]=\frac{dp_0}{dt}+p_0\tau_0{}'+\\ \sum_{n=1}^{\infty}\frac{\tau_n{}'p_n}{2}+\frac{1}{x_2-x_1}\sum_{n=1}^{\infty}p_n[\frac{dx_1}{dt}-(-1)^n\frac{dx_2}{dt}]\\ \text{where:}\\ \frac{\partial p}{\partial x}|_{x1}=\frac{1}{2qA}(\frac{I_{n1}}{D_n}-\frac{I_{p1}}{D_p});\\ \frac{\partial p}{\partial x}|_{x2}=\frac{1}{2qA}(\frac{I_{n2}+I_{imp}}{D_n}-\frac{I_{p2}}{D_p})\end{cases}\tag{15}$$

Calculation of the Fourier coefficients of τ_k' is achieved by finding the inverse of the original Fourier series expression [24]:

$$\begin{bmatrix}\tau'_0(t)\\ \tau'_1(t)\\ \tau'_2(t)\\ \vdots\end{bmatrix}=inv([\begin{matrix}1 & 1 & 1 & \cdots\\ 1 & \cos(\frac{\pi}{M-1}) & \cos(\frac{2\pi}{M-1}) & \cdots\\ 1 & \cos(\frac{2\pi}{M-1}) & \cos(\frac{4\pi}{M-1}) & \cdots\\ \vdots & \vdots & \vdots & \ddots\end{matrix}])\cdot\begin{bmatrix}\tau'_0(x_1,t)\\ \tau'_1(x_1+\Delta x,t)\\ \tau'_2(x_1+2\Delta x,t)\\ \vdots\end{bmatrix}\tag{16}$$

The total voltage drop across the CSR, V_{CSR}, is derived using the same method in [14]. The junction voltage of J2 is given by depletion region voltage in the next section.

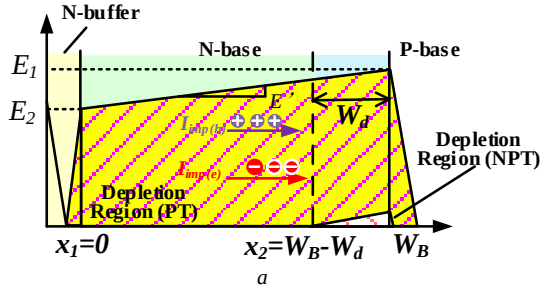

a

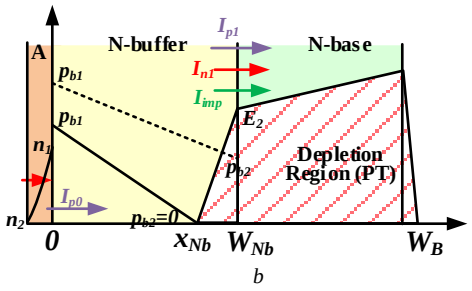

b

Fig. 3. *The Layout of the Depletion Region and the N-buffer Region*

(a) The depletion region arrangement in the IGCT base area during punch-through (PT) and non-punch-through (NPT).
(b) Boundary conditions of the N-buffer region

3.4. Model of the Depletion Region with Impact Ionization Effect

The equilibrium concentration at P-N junction is used to derive the depletion region voltage:

$$V_d=-V_t\ln(\frac{N_Bp_{x2}}{n_i^2})\tag{17}$$

The expansion of the depletion region is shown in Fig. 3 (a). The simplest way to model the depletion region is to derive the width of depletion region (W_d) from the forward blocking voltage (V_d) and electric field gradient (E'). Due to the high doping profile in P-base, the part of depletion region in the P-base region is neglected. Thus W_d and the moving boundary of CSR, x_2, can be expressed as:

$$\begin{cases}W_d=\begin{cases}\sqrt{2V_d/E'} & V_d\le E'W_B^2/2\\ W_B & otherwise\end{cases}\\ x_2=\begin{cases}W_B-W_d & V_d\le E'W_B^2/2\\ 0 & otherwise\end{cases}\end{cases}\tag{18}$$

Hence the blocking voltage V_d is allowed to increase with W_d limited to W_B. The boundary electric field, E_1 and E_2, can be derived as:

$$\begin{cases}E_1=\begin{cases}E'W_d & W_d\le W_B\\ \frac{V_d}{W_B}+\frac{W_BE'}{2} & otherwise\end{cases}\\ E_2=\begin{cases}0 & W_d\le W_B\\ E_1-E'W_d & otherwise\end{cases}\end{cases}\tag{19}$$

The displacement current at the P-base end of the depletion region is:

$$I_{disp}=\varepsilon_{Si}A\frac{dE_1}{dt}\tag{20}$$

which is one of the current components as the boundary condition for the P-base region model.

Thus the only variable needs to be solved in model (18)-(20) is the electric field gradient, E'. The derivation of E' is coupled with the impact ionization effect which plays an important role in limiting the peak forwards voltage during turning off. Impact ionization is governed by [25]:

$$G = -\frac{|J_p + J_n|}{q}\alpha \tag{21}$$

$$\begin{cases} \alpha = \alpha_0 \exp(\frac{b_i}{E_{cri}^2}E - \frac{b_i}{E_{cri}}) \\ \alpha_0 = A_i \exp(-\frac{b_i}{E_{cri}}) \\ A_i = 1.07\times10^6\,\mathrm{cm}^{-1} \\ b_i = 1.65\times10^6\,\mathrm{Vcm}^{-1} \\ E_{cri} = 1.9\times10^5\,\mathrm{Vcm}^{-1} \end{cases}$$

where α is the number of holes and electrons generated per unit distance by the impact ionization process, E_{cri} is the critical electric field in the depletion region. The parameters are not normalized here for explicit illustration.

Fig. 3 (a) shows the impact ionization current (I_{imp}) in the depletion region. Generated holes are swept at saturated velocity towards the P-base, while generated electrons towards the N-buffer. This gives a reduced electric field gradient:

$$E' = \frac{qN_B}{\varepsilon_{Si}} + \frac{|I_{p2}|}{\varepsilon_{Si}Av_{sat}} - \frac{|I_{imp}|}{\varepsilon_{Si}Av_{sat}} \tag{22}$$

Solution of I_{imp} proceeds as in [25]. (21) is substituted into the continuity equation. Assuming the gradient of hole and electron concentration at boundary is zero, the current generated by impact ionization is given as:

$$\begin{cases} I_{imp} = m_0 I_{p2} \Big/ (\dfrac{m_1 E'}{\alpha_0 \exp(m_1E_2 - m_2)(\exp(m_1E_1'W_d) - 1)} - 1) \\ \text{where } m_1 = \dfrac{b_i}{E_{cri}^2},\ m_2 = \dfrac{b_i}{E_{cri}} \end{cases} \tag{23}$$

where m_0=1.3 is chosen so that this expression matches the exact solution. Thus, combining (17)-(20), (22) and (23), the model for the depletion region is obtained. To avoid the discontinuity problem caused by the algebraic loop, a time lag equal to $2W_d/v_{sat}$ is applied to I_{imp} when modelling the depletion region model. The applied time lag also exists in the real device because the holes and electrons, generated by impact ionizations, take an approximate interval of $2W_d/v_{sat}$ to be swept out of the depletion region.

The boundaries of CSR are shown in Fig. 3(a). When PT occurs, the width of the CSR ($w=x_2-x_1$) is limited to approximately one diffusion length because w is not allowed to drop to zero in the proposed Fourier series method. The diffusion length is calculated from mobility related to electric field [24]:

$$\begin{cases} \mu_{n,p} = \dfrac{\mu_{n0,p0}}{[1 + (\mu_{n0,p0}|E_1 + E_2| \Big/ 2v_{sat})^{\beta}]^{1/\beta}} \\ L_a = \sqrt{\dfrac{2\tau_{HL}V_t\mu_n\mu_p}{\mu_n + \mu_p}} \end{cases} \tag{24}$$

where $\beta=1$ for holes and $\beta=2$ for electrons. Also, the limitation of the width w during PT applies only to the Fourier series ADE solution. The electric field, depletion layer widths and voltages are still calculated with $x_1=x_2$.

3.5. Model of the N-buffer Region with Moving Boundary

Since the N-buffer layer is highly doped and thin compared to the N-base region, the N-buffer region can be modelled with the same equations as the P-base region. The boundary conditions of N-buffer region is shown in Fig. 3 (b).

Applying the continuity equation to the N-buffer region, the model of the N-buffer region can be expressed as:

$$\begin{cases} \dfrac{dQ_{Nb}}{dt} = -\dfrac{Q_{Nb}}{\tau_L} + I_A - I_{n0} - I_{p1} - I_E \\ I_E = \dfrac{1}{2}\dfrac{p_{b1}}{x_{Nb}}\dfrac{dx_{Nb}}{dt} \\ Q_{Nb} = \dfrac{qAx_{Nb}(p_{b1} + p_{b2})}{2} \\ I_{p1} = \dfrac{qAD_p(p_{b1} - p_{b2})}{x_{Nb}} \\ p_{b2} = \dfrac{p_{x1}^2}{N_{Nb}} \\ I_{n0} = \dfrac{qAD_n p_{b1}^2}{L_n \tanh(W_{anode}/L_n)} \quad (L_n = \sqrt{\tau_n D_n}) \end{cases} \tag{25}$$

where Q_{Nb} is total excess carriers in the N-buffer region. I_{p1} is the diffusion component of the total hole current. I_E is introduced into the equation to explain the boundary electric field sweep-out effect on the excess carriers when PT happens. I_{n0} is the recombination current in the transparent anode. It is derived by the same method as (9).

For the N-buffer is thin, the moving boundary due to E_2 can't be neglected. The effective width of the N-buffer region is modeled by x_{Nb}:

$$x_{Nb} = \begin{cases} W_{Nb} & W_d \le W_B \\ W_{Nb} - E_2 \Big/ (qN_{Nb}/\varepsilon_{Si} - I_{imp}/\varepsilon_{Si}Av_{sat}) & otherwise \end{cases} \tag{26}$$

To ensure general applicability of the model, I_{imp} is added to the total electron current to give accurate electric field gradient.

Therefore, (25) and (26) link the N-buffer layer to the depletion region and the N-base region.

The voltage drop across the N-buffer region comprises two components: the voltage drop across J1 and the voltage drop across the boundary of the N-buffer region adjacent to the CSR, (27).

$$\begin{cases} V_{J1} = V_t \ln(\dfrac{p_{b1}N_{Nb}}{n_i^2}) \\ V_{Nb} = V_{J1} + V_t \ln(\dfrac{N_B}{N_B + p_{x1}}) \end{cases} \tag{27}$$

The gated drive is simplified by applying a DC voltage source connected in series with a resistor and an inductor, of which the value is 0.08 mΩ and 2.15 nH respectively [12].

4. Model Implementation

4.1. Model Implementation in Simulink

The Fourier series must be truncated in order to be implemented practically. The number of terms (M) will

depend on the ambipolar diffusion length (L_a) relative to the base region width W_B, as $M = W_B/L_a$ [24]. For high power IGCTs, W_B is in the range of 300-800 μm which is significantly larger than L_a. In this paper, M=15 is found to be acceptable for both accuracy and calculation time.

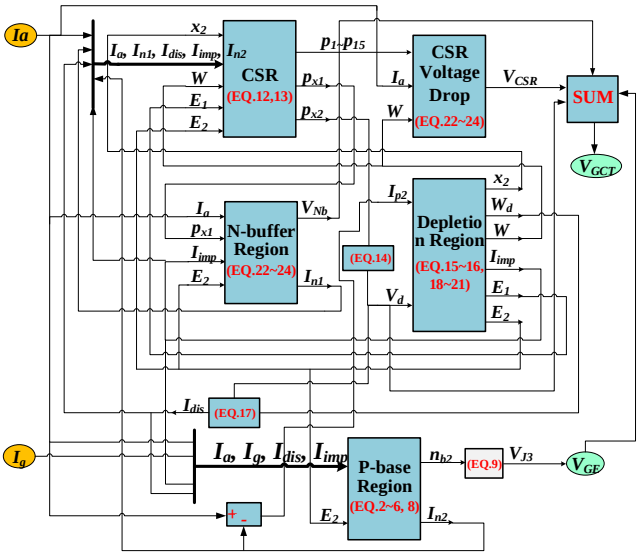

Fig. 4 . *Implementation of Proposed Physics-Based Compact Model In Simulink*

The proposed IGCT model is implemented using the MATLAB/Simulink. Each mathematical equation is represented by the transfer function provided by the software. Implementation of the ADE solution in Simulink requires the use of a stiff solver due to the widely differing time constants present in the model. Suitable solvers are ode15s and ode23tb; these are similar to Gear's method used in PSpice circuit simulator. The solver ode23tb has been found to give the most stable result. The maximum step size is 10^{-6}s. The relative tolerance is 10^{-3} and the absolute tolerance is 10^{-4}. In addition, the simulator advanced options are set to use inline parameters and zero crossing detection is switched off to improve the execution speed. The outline block diagram of the Simulink Model is shown in Fig. 4.

4.2. Comparison with Level-4 model Developed in Silvaco Atlas

Table.3 Models and Computing settings

	Settings	
	Atlas	**Proposed Model**
Main Models	Concentration and field dependent mobility; Impact ionization; Carrier-carrier scattering model	Eq.(1)-(25)
Dimension	2	1
Mesh or grid	23348 triangles 47892 points	M=15
Local Truncation Error (LTE)	10^{-3}	10^{-3}
Relative Tolerance	10^{-5}	10^{-4}
Iteration Method	Newton-Raphson algorithm	Ode23
Simulation implementation	One pulse switching	

The proposed model was first compared with Level-4 model developed in Silvaco Atlas. The parameters of GCT applied in simulation are in consistent with the IGCT of 5SHY 42L6500 used in the experiment of the next section. The computing setting details of both proposed model and Atlas model are summarized in Table.3 in order to make comparison.

Results are shown in Fig. 5. Fig. 5 (a) shows the transient results and Fig. 5 (b) shows the excess carrier concentration throughout the N-base and N-buffer region during turning off.

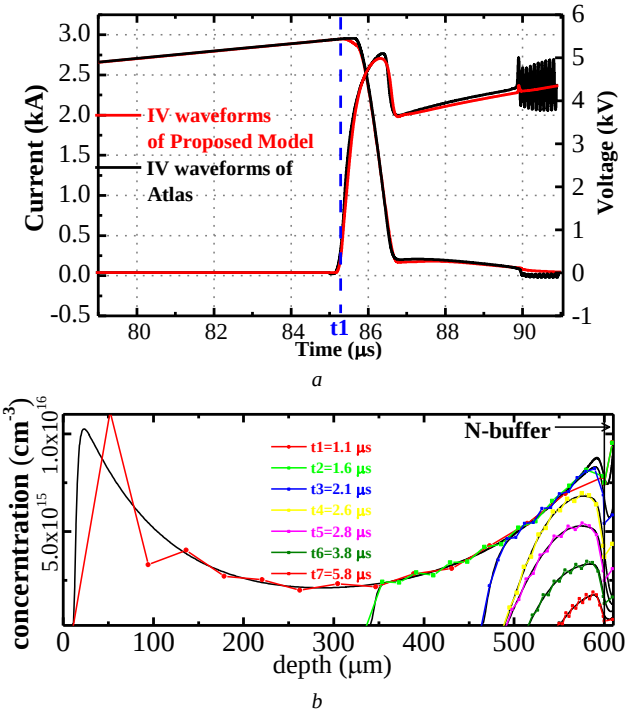

Fig. 5 . *Waveforms and hole concentration during turn-off from Atlas and Simulink simulation.*

(a) Cathode current, anode current and anode voltage waveforms.

(b) Hole concentration from t1=1.1 μs since turn-off begins, t1 in (b) is also marked in (a).

The agreement between the proposed compact model and Atlas is excellent. By using the Fourier series method, the excess carrier concentration in the N-base region matches well with the accurate results solved from ADE. The oscillation in the Atlas voltage waveform in Fig. 5 (a) is a numerical oscillation at the end of turning off due to the meshing problem. The specification of the meshes in Atlas involves a trade-off between the requirements of accuracy and computing speed. Good precision requires fine mesh. However, high simulation speed requires loose mesh that minimizes the total number of the grid points. According to the users' guide of Silvaco Atlas, ideally the variations of electric potential across an element of grid shall be limited to no more than *Vt*, which is 0.025875V. In high voltage IGCT, the N-base area is very thick, and the maximum electric field approaches the critical electric field, *Ecri*, when blocking high voltage. Following such a meshing specification, the width of the grid in most of the depletion region should be about $Vt/Ecri \approx 0.1\mu m$. As the dimension parameters indicated in Table 4, excessively large number of grids are required in the depletion region of the high voltage IGCT, which would in practice often exceeds the upper limit of grid points allowance in Silvaco. Therefore, a meshing grid of reduced density is essential in practice. Regarding the Silvaco simulations in this paper, the rounding issue due to a moderated meshing grid

only affects the ending part of simulation, which is in the nominal off-state where high contrast of carrier concentration exists within the device. Since the focus here is in the turn-off transient, the rounding issue does not affect the validation of the modelling work in this paper.

However, the numerical oscillation of voltage when switching off can be practically eliminated in this compact model for there is no meshing problem using the simplified depletion region model.

The comparison with Atlas shows that the proposed model provides accurate prediction of IGCT's transient behavior but in a significantly faster computing speed. The computing time of proposed model is **1.67s**. However, the computing time of Atlas is no less than **5 hours.**

5. Experimental Validation

5.1. Experimental Parameters

The proposed model was verified with two types of IGCTs manufactured by the ABB company, of which the rated voltage and current are different. The doping profile parameters are extracted using the spread resistance probe (SRP). The SRP method is a technique for determining the doping profile by measuring the local silicon resistivity along the cross section of the GCT's silicon wafer. More details can be found in reference [26] and [27].

And the lifetime parameters are extracted through on-state voltage drop compared to datasheet as well as tail currents compared to experiments. The parameters are summarized in Table.4.

Table.4 Model Parameters Used for Validation

Parameters	IGCTs	
	5SHY 42L6500	5SHY 55L4500
W_B/cm	600×10^{-4}	385×10^{-4}
W_{Pb}/cm	120×10^{-4}	120×10^{-4}
W_{Nb}/cm	30×10^{-4}	25×10^{-4}
N_{Pb}/cm^{-3}	10^{17}	10^{17}
N_B/cm^{-3}	10^{13}	2×10^{13}
N_{Bb}/cm^{-3}	10^{16}	10^{16}
τ_{HL}/μs	10	10
τ_L/μs	1	1
m_t	0.18	0.15

The turn-off waveforms of IGCTs were used for comparison. The turn-on waveform has not been presented for the turn-on and on-state characteristics have already been verified by previous work in [14]. In addition, the physical improvements applied to our model are focused on transient phenomenon during turning off.

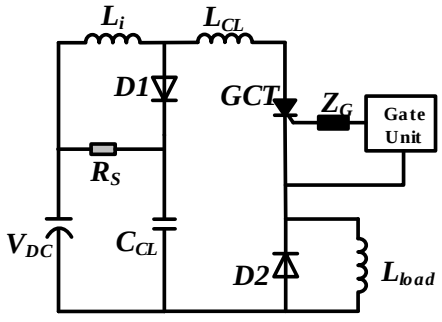

a

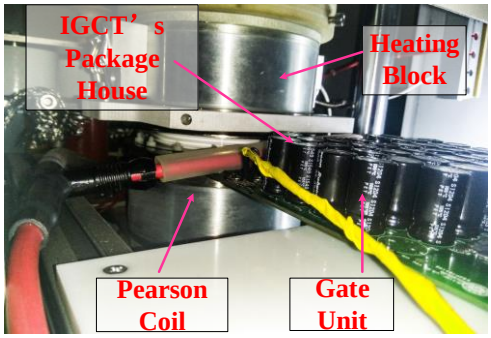

b

Fig. 6. (a)*Layout of Test Circuit,* ***(b)****Experiment Platform*

The layout of test circuit and the experiment platform is shown in Fig. 6. A Pearson coil and a differential probe were used to measure the anode current and voltage, respectively. A heating clamp was used to maintain the ambient temperature. The parameters of the experiment platform are summarized in Table.5.

Table.5 Parameters of Experiment Platform

Parameters	Value
C_{CL}	10 μF
R_s	0.65 Ω
L_i	5 μH
L_{CL}	0.3 μH
L_{load}	78 μH
Temperature	300K

5.2. Comparison with Experimental Results

Comparison between experiment and simulation in turn-off waveforms using 5SHY 42L6500 is shown in Fig. 7. Experiments with different voltage and current were carried out. The model proposed in this paper and mentioned in [14] are both applied to the IGCT for comparison. The larger current waveform in Fig. 7 (a) and Fig.7 (b) corresponds to the larger anode voltage waveform in Fig. 7 (c) and Fig.7 (d).

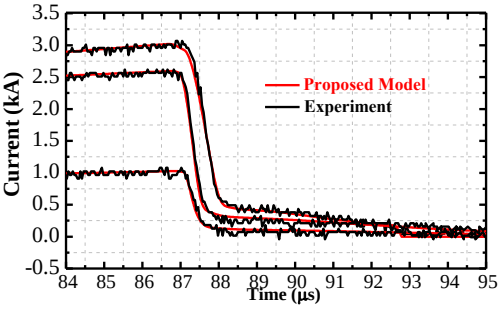

a

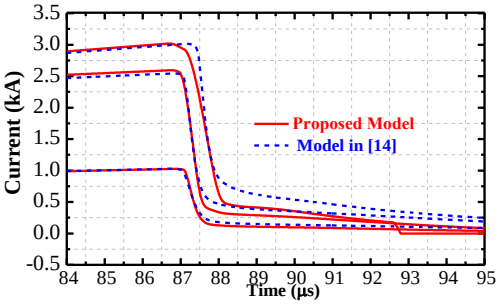

b

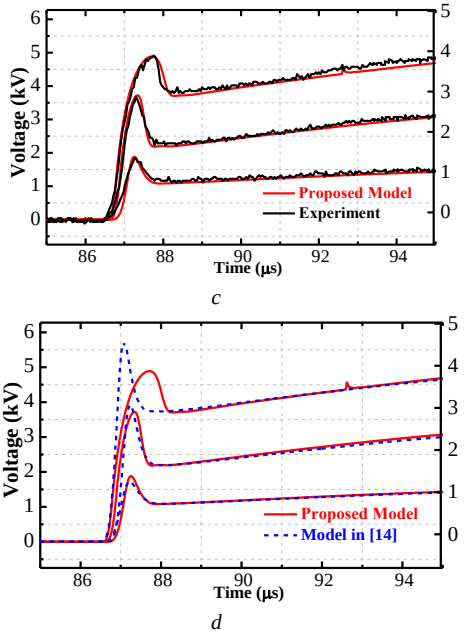

Fig. 7 . *Comparison between experiment and simulation waveforms with different DC voltage and load current. IGCT type: 5SHY 42L6500:*
(a) Anode currents of proposed model and experiments
(b) Anode currents of proposed model and model in [14].
(c) Anode voltages of proposed model and experiments.
(d) Anode voltages of proposed model and model in [14].

The IGCT of type 5SHY 42L6500 has a rated overvoltage of 6.5kV, of which the thickness of N-base region is no less than 600 μm. When turning off, the excess carriers in the CSR will result in a slow decay of the anode current, referred to the current tail. The local lifetime region is applied to shorten the time of current tail decay. As shown in Fig. 7 (a), the tail current modelled with local lifetime region has capability of simulating the current tail decay, showing an accurate match to the experimental results at different current. The model without local lifetime region, by contrast as blue dashed lines in Fig. 7 (b), has incapability of modelling the current tail at high current, resulting in a discrepancy between the modelling and real behavior.

The anode voltage rise also matches well with the experiment under different voltage level. By introducing the impact ionization effect equations, the proposed model demonstrates an enhanced accuracy of predicting the IGCT' anode voltage behavior as shown in Fig. 7 (c) compared to blue dashed lines in Fig. 7 (d), especially at higher blocking voltage.

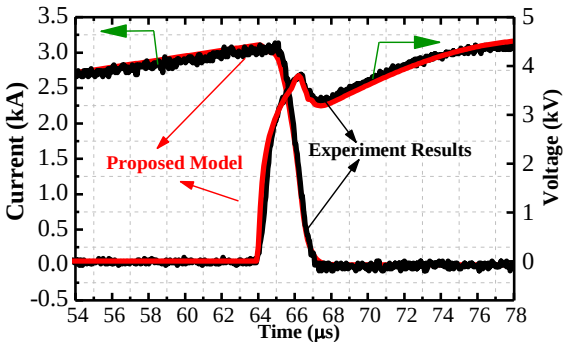

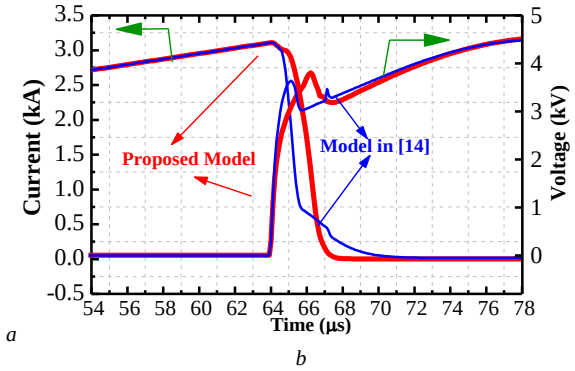

Fig. 8 . *Simulation results of proposed model and model in* [14] *compared to experiment results.*
(a) Anode currents and voltages of proposed model and experiment results.
(b) Anode currents and voltages of proposed model and model in [14].

We tested the other IGCT, 5SHY 55L4500 to verify the current tail during PT. This is because the rated voltage of this 5SHY 55L4500 is 4.5 kV, corresponding to a thinner N-base region compared to the 5SHY 42L6500. So with the same DC voltage, it is easier to test the PT phenomenon with type 5SHY 55L4500. The experiment of 2.8 kV/3 kA was carried out. Fig. 8 shows the comparison of voltage and current waveforms when turning off. Good enhancement is obtained with the newly developed model compared to previous work. The current waveform shows better agreement especially in the current tail when PT happens.

The proposed compact model agrees well with the real device behavior demonstrated by comparison with the experimental results with two types of IGCT. The introduction of local lifetime region in this compact model has resulted in a significant shorter and lower current tail. In addition, the introduction of impact ionization effect mainly modified the anode voltage rise waveform. This is because the generated holes reduce the electric field gradient in the depletion region. Both the moving boundary effect and electrical field sweep-out effect have been considered in the N-buffer region, resulting in a rapid fall in the current tail.

6. Conclusion

The proposed compact model of IGCT has clearly captured the effect of impact ionization, local lifetime region and moving boundary of N-buffer region when punch-through happens, during the transient process of turning off. The impact ionization effect mainly modifies the anode voltage rise waveform in high power application, leading to better prediction of switching loss and overvoltage when turning off. The modified Fourier series method considering the local lifetime region has results in a significant shorter and lower current tail, agreed well with the experiment results. And the moving boundary of N-buffer region when PT happens has also enhanced the current agreement. The prediction of voltage and current waveform shows that this newly developed level 3 model offers a similar accuracy to level 4 model. However, it offers a significantly faster calculation speed, allowing its application in the system level circuit simulation and the GCT wafer's lateral optimization.

7. Reference

[1] Ladoux, P., Serbia, N., Carroll, E I.: 'On the Potential of IGCTs in HVDC', IEEE Journal of Emerging and Selected Topics in Power Electronics, 2015, 3.3, pp. 780-793.

[2] Wahlstroem, J., Dujic, D., Luescher, M A., et al.: 'High power IGCT based multilevel inverter'. Proc. Int. Conf. International Exhibition and Conference for Power Electronics, Intelligent Motion, Renewable Energy and Energy Management, Nuremberg, Germany, May, 2014, pp. 1-6.

[3] Vemulapati, U., Rahimo, M., Arnold, M., et al.: 'Recent advancements in IGCT technologies for high power electronics applications'. Proc. Int. Conf. Power Electronics and Applications (EPE'15 ECCE-Europe), Geneva, Switzerland, September, 2015, pp, 1-10.

[4] Agostini, F., Vemulapati, U., Torresin, D., et al.: '1MW bi-directional DC solid state circuit breaker based on air cooled reverse blocking-IGCT'. Proc. Int. Conf. Electric Ship Technologies Symposium (ESTS), Old Town Alexandria, America, June, 2015, pp, 287-292.

[5] Budihardjo, I., Lauritzen, P. O., Wong, K. Y., et al.: 'Defining standard performance levels for power semiconductor devices'. Proc. Int. Conf. Industry Applications Conference, Thirtieth IAS Annual Meeting, Orlando, Florida, USA, October, 1995, pp, 1084-1090.

[6] Santi, E., Hudgins, J. L., Mantooth, H. A., 'Variable model levels for power semiconductor devices'. Proc. Int. Conf. The 2007 Summer Computer Simulation Conference, San Diego, USA, July, 2007, pp, 276-283.

[7] C. Alonso., T. A. Meynard., H. Foch., et al.: 'A model of GTO compatible with power circuit simulation', Proc. Int. Conf. 1993 Fifth European Conference on Power Electronics and Applications, Brighton, UK, 1993, pp, 232-237.

[8] YUAN L., ZHAO Z., Bai H., et al.: 'The functional model of IGCTs for the circuit simulation of high-voltage converters'. Proc. Conf. Chinese Society for Electrical Engineering, Beijing, October, 2004, 6: 012.

[9] Ma, C, L., Lauritzen, P, O., Lin, P, Y., et al.: 'A systematic approach to modeling of power semiconductor devices based on charge control principles'. Proc. Int. Conf. Power Electronics Specialists Conference, Taibei, Taiwan, June, 1994, pp, 31-37.

[10] Ma, C. L., Lauritzen, P. O., Sigg, J,.: 'A physics-based GTO model for circuit simulation'. Proc. Int. Conf. 26th Annual IEEE Power Electronics Specialists Conference, Atlanta, USA, June, 1995, pp, 872-878.

[11] Palmer, P. R., K. J. Tseng.,: 'An accurate GTO model for circuit simulations'. Proc. Int. Conf. Fifth European Conference on Power Electronics and Applications, IET, Brighton, UK, September, 1993, pp, 244-248.

[12] Lyu, G., Yu, Z., Zeng, R., et al: 'Optimization of gate-commutated thyristors for hybrid DC breakers'. IET Power Electronics, 2017, 10(14), pp, 2002-2009.

[13] Bryant, A, T., Palmer, P, R., Santi, E., et al.: 'Simulation and optimization of diode and insulated gate bipolar transistor interaction in a chopper cell using MATLAB and Simulink'. IEEE Transactions on Industry Applications, 2007, 43(4), pp, 874-883.

[14] Wang, X., Caiafa, A., Hudgins, J. L., et al.: 'Implementation and validation of a physics-based circuit model for IGCT with full temperature dependencies'. Proc. Int. Conf. Power Electronics Specialists Conference, Aachen, Germany, June, 2004, Vol. 1, pp, 597-603.

[15] Metzner, D., Schroder, D.: 'A physical GTO model for circuit simulation'. Proc. Int. Conf. Industry Applications Society Annual Meeting, Houston, USA, October, 1992, pp, 1066-1073.

[16] Kuhn, H., Schroder, D.: 'A new validated physically based IGCT model for circuit simulation of snubberless and series operation'. IEEE Transactions on Industry Applications, 2002, 38(6), pp, 1606-1612.

[17] Tseng K J, Palmer P R.: 'Mathematical model of gate-turn-off thyristor for use in circuit simulations'. IEE Proceedings-Electric Power Applications, 1994, 141(6), pp, 284-292.

[18] Kang, X., Caiafa, A., Santi, E., et al.: 'Characterization and modeling of high-voltage field-stop IGBTs'. IEEE Transactions on Industry Applications, 2003, 39(4), pp, 922-928.

[19] Vemulapati, U., Arnold, M., Rahimo, M., et al.: 'An experimental demonstration of a 4.5 kV “Bi-mode Gate Commutated Thyristor”(BGCT)'. Proc. Int. Conf. IEEE 27th International Symposium on Power Semiconductor Devices & IC's (ISPSD), Hong Kong, China, May, 2015, pp, 109-112.

[20] Lophitis, N., Antoniou, M., Udrea, F., et al.: 'The destruction mechanism in GCTs'. IEEE Transactions on Electron Devices, 2013, 60.2, pp, 819-826.

[21] De Mari, A.: 'An accurate numerical one-dimensional solution of the pn junction under arbitrary transient conditions'. Solid-State Electronics, 1968, 11(11), pp, 1021-1053.

[22] Stiasny, Thomas., Bjoern, Oedegard., Eric, Carroll.: 'Lifetime engineering for the next generation of application-specific IGCTs'. Drives & Controls, London, UK, 2001.

[23] Oedegard, B., Stiasny, T., Carroll, E., et al.: 'An application specific asymmetric IGCT'. Proc. Int. Conf. Power Electronics Conference Presented at Power Systems World 2001 Conference and Exhibition, Rosemont, USA, November, 2003, pp, 283-290.

[24] Bryant, A. T., Lu, L., Santi, E., et al.: 'Physical modeling of fast pin diodes with carrier lifetime zoning, part I: Device model'. IEEE transactions on power electronics, 2008, 23(1), pp, 189-197.

[25] Göhler, L., Sigg, J.: 'Analytical model for dynamic avalanche breakdown in power devices'. Proc. Int. Conf. European Conference on power electronics and applications, Trondheim, Norway, September, 1997, Vol.4, pp, 4-129.

[26] Mazur, R, G., Dickey, D, H.: 'A spreading resistance technique for resistivity measurements on silicon'. Journal of the electrochemical society, 1966, 113(3), pp, 255-259.

[27] Snauwaert, J., Hellemans, L., Czech, I., et al.: 'Towards a physical understanding of spreading resistance probe technique profiling'. Journal of Vacuum Science & Technology B: Microelectronics and Nanometer Structures Processing, Measurement, and Phenomena, 1994, 12(1), pp, 304-311
.